Electronic signature of the vacancy ordering in NbO (Nb_3O_3)

A. K. Efimenko,[1] N. Hollmann,[1] K. Hoefer,[1] J. Weinen,[1] D. Takegami,[1] K. K. Wolff,[1] S. G. Altendorf,[1] Z. Hu,[1] A. D. Rata,[1] A. C. Komarek,[1] A. A. Nugroho,[2] Y. F. Liao,[3] K.-D. Tsuei,[3] H. H. Hsieh,[4] H.-J. Lin,[3] C. T. Chen,[3] L. H. Tjeng,[1,*] and D. Kasinathan[1,†]

[1]*Max Planck Institute for Chemical Physics of Solids, Noethnitzer Strasse 40, 01187 Dresden, Germany*

[2]*Insitiut Teknologi Bandung, Jalan Ganesha 10, 40132 Bandung, Indonesia*

[3]*National Synchrotron Radiation Research Center (NSRRC), 101 Hsin-Ann Road, 30076 Hsinchu, Taiwan*

[4]*Chung Cheng Institute of Technology, National Defense University, Taoyuan 335, Taiwan*

(Received 4 August 2017; revised manuscript received 18 October 2017; published 6 November 2017)

We investigated the electronic structure of the vacancy-ordered 4*d*-transition-metal monoxide NbO (Nb_3O_3) using angle-integrated soft- and hard-x-ray photoelectron spectroscopies as well as ultraviolet angle-resolved photoelectron spectroscopy. We found that density-functional-based band-structure calculations can describe the spectral features accurately provided that self-interaction effects are taken into account. In the angle-resolved spectra we were able to identify the so-called 'vacancy' band that characterizes the ordering of the vacancies. This together with the band-structure results indicate the important role of the very large inter-Nb-4*d* hybridization for the formation of the ordered vacancies and the high thermal stability of the ordered structure of niobium monoxide.

DOI: 10.1103/PhysRevB.96.195112

I. INTRODUCTION

The transition-metal (TM) monoxide NbO is special. Although many transition-metal monoxides adopt the highly dense rock-salt crystal structure, NbO, synthesized already more than 150 years ago [1], crystallizes in a structure in which 25% of the Nb and 25% of the O ions are removed from the rock-salt lattice. The Nb and O vacancies are ordered, and there are no additional distortions of the lattice [2–4], see Fig. 1. For clarity, the hypothetical rock salt and the actual vacancy-ordered crystal structure of niobium monoxide will be referred to as Nb_4O_4 and Nb_3O_3, respectively. Adding to the astonishment, the vacancy order is robust, and the crystal structure remains stable up until 2213 K, the melting point of niobium monoxide [3,5–8].

Although the formation of defects or vacancies in either the cation or the anion sites is in itself not a rare phenomenon for TM oxides [9–11], the precise and robust ordering of the vacancies in niobium monoxide give perhaps credit to efforts that treat its crystal structure not so much as a defect problem but as a three-dimensional network of corner-sharing condensates of Nb_6O_{12} clusters. This is motivated by the analogy with the TM_6X_{12} clusters that form Chevrel phases (X = halogen, chalcogen, or pnictide) [10,12,13]. Figure 1 (right) gives an illustration of such a building block.

Density-functional-based band-structure calculations have been performed [12,14–16] to explain the properties of niobium monoxide [17–20], and it was found that the Nb_3O_3 structure is more stable than the Nb_4O_4 structure by about 1 eV per NbO unit [15,16]. Our objective here is to test experimentally the accuracy of the band-structure calculations and to identify the bands in the measured spectra that are characteristic for Nb_3O_3 thereby proving that the vacancies are ordered and that band formation is an essential ingredient for the formation of vacancies in niobium monoxide.

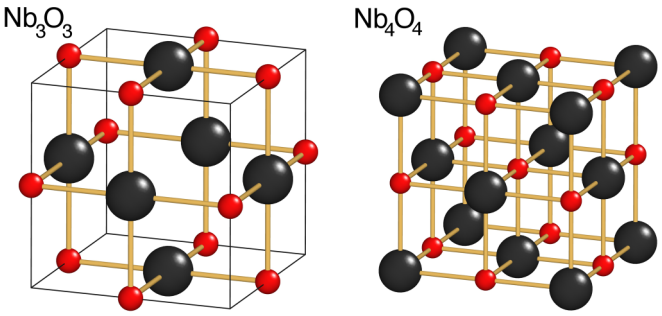

FIG. 1. Crystal structure of the standard rock-salt lattice (left) and the long-range vacancy-ordered rock-salt lattice with one quarter of the atoms missing from both sublattices (right). The large and small spheres depict niobium and oxygen atoms, respectively. Niobium monoxide in the hypothetical rock-salt structure is labeled as Nb_4O_4 and in the real vacancy-ordered structure is labeled as Nb_3O_3.

II. METHODS

Angle-integrated photoelectron spectroscopy measurements have been carried out at three facilities: (1) the Dragon beamline 11A at the National Synchrotron Radiation Research Center (NSRRC) in Taiwan with the energy of the soft x rays set to $h\nu = 700$ eV, (2) at the Max-Planck-Institute photoemission facility in Dresden having a monochromatized Al-$K_\alpha h\nu = 1486.6$ eV x-ray source, and (3) at the Max-Planck-NSRRC hard x-ray photoelectron spectrosopy (HAXPES) end station [21] at the Taiwan undulator beamline BL12XU of SPring-8 in Japan with the photon energy set to $h\nu = 6.5$ keV. The photoemission facilities in Taiwan (1) and Japan (3) were equipped with MB Scientific A-1 electron energy analyzers, and the one in Dresden (2) was equipped

*hao.tjeng@cpfs.mpg.de
†deepa.kasinathan@cpfs.mpg.de

with a VG Scienta R3000. Angle-resolved photoelectron spectroscopy (ARPES) was performed at the (1) NSRRC Dragon beamline 11A with the photon energies varied between 90 and 185 eV in order to cover the fifth Brillouin zone of niobium monoxide. Single crystals of niobium monoxide were grown by the traveling-solvent floating zone method. The samples were *ex situ* aligned using a Laue camera and cleaved *in situ* under ultrahigh vacuum conditions. The [001] crystal direction is set at normal emission to the electron analyzer lens opening.

The electronic structure calculations were performed using WIEN2K, an augmented plane wave plus local orbitals program [22]. Two kinds of parametrization of the exchange-correlation potential were employed: the Perdew, Burke, and Ernzerhof (PBE) parametrization within the generalized gradient approximation (GGA) [23] and a screened hybrid functional for all the electrons [24–26]. The screened hybrid functional (E_{xc}^{hybrid}) was constructed such that a part (α) of the semilocal PBE-GGA exchange (E_x^{GGA}) was replaced by the short-range part of the Hartree-Fock exchange (E_x^{HF}) according to

$$E_{xc}^{\text{hybrid}} = \alpha E_x^{\text{HF}} + (1-\alpha)E_x^{\text{GGA}} + E_c^{\text{GGA}}, \qquad (1)$$

where E_c^{GGA} is the correlation energy. We varied α from 0 to 0.3, and the best fit was found for $\alpha = 0.14$ as will be shown below. The Brillouin zone was sampled by a well-converged mesh of 5000 k points in the full zone. The experimental lattice constant $a = 4.21$ Å has been used throughout [4].

III. RESULTS

A. Valence-band photoemission spectra

Figure 2 displays the valence-band (VB) photoemission spectra of niobium monoxide taken with $h\nu =$ 700, 1486.6 eV, and 6.5 keV photon energies. The 700 eV spectrum was taken at room temperature with an overall energy resolution of 0.7 eV, the 1486.6 eV spectrum was taken at room temperature with 0.4 eV resolution, and the 6.5 keV spectra were taken at 80 K with 0.17 eV resolution. All spectra are normalized to their integrated intensities after the subtraction of the standard integral background to account for inelastic-scattering processes [27]. All the spectra show a clear cutoff at zero energy (E_F, Fermi level), consistent with the system being a good metal [17,28–30]. All spectra are comparable to one another in terms of the total bandwidth and peak positions, affirming their intrinsic nature. The intensities of the spectral features vary with photon energy, reflecting the photon energy dependence of the photoionization cross sections of the atomic orbitals contributing to the VB: Nb-4d, O-2p, and Nb-5s [31–34].

We have used two different geometries for the 6.5 keV spectra. In the so-called horizontal geometry, the electron energy analyzer was mounted horizontally and parallel to the electrical-field vector of the photon beam, whereas in the vertical geometry, it is perpendicular to the electrical-field vector and the Poynting vector of the beam [21]. The spectral intensities depend strongly on the polarization of the light and are given by the so-called β-asymmetry parameter

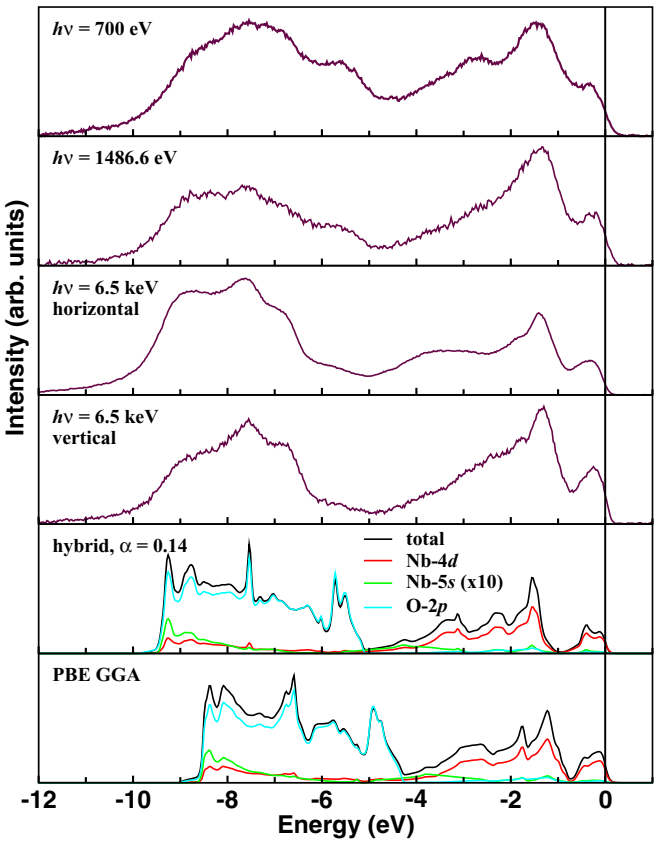

FIG. 2. Valence-band spectra of niobium monoxide taken with photon energies $h\nu = 700, 1486.6$ eV, and 6.5 keV together with the total and orbital projected partial density of states calculated using the hybrid functional and PBE-GGA exchange-correlation functional.

of the photoionization cross sections of the various atomic shells involved [31–34]. In particular, it has been shown experimentally [21] that the s contribution to the spectra is substantially reduced in the vertical geometry. The differences in the 6.5 keV spectra for the two geometries thus give an indication for the energy distribution of the Nb-5s states.

VB photoemission spectra have been reported previously for very low-energy incident photons with $h\nu = 30$, 68, and 83.8 eV [18,19]. Considering the enormous energy difference of the incident photons with the present experiments, the peaks around -1.5 and -7 eV energies along with a shoulder around -5.5 eV are qualitatively similar with those earlier reports [18,19]. Yet, we are now able to discern additional features due to the improved energy resolution and larger variation of the photoionization cross sections, which help us to present a more precise analysis of the electronic structure of niobium monoxide as discussed below.

We begin by comparing the experimental VB spectra with the calculated density of states (DOS) for Nb_3O_3 using the PBE-GGA exchange-correlation functional (Fig. 2, bottom panel). To facilitate an easy comparison, the calculated DOS was multiplied with the Fermi function. At first glance, the general features of the experimental data seem to be reproduced by these calculations with the spectral weight closest to

the Fermi level (0 to −4 eV) originating mainly from Nb-4*d* states, whereas the spectral weight at deeper energies (−5 to −10 eV) are an admixture of Nb-4*d* and O-2*p* states. On closer inspection, certain discrepancies emerge: First and foremost, the widths of the measured spectra (∼10 eV) are larger than the calculations (∼8.5 eV) thereby reducing the separation between the centers of the Nb-4*d*- and O-2*p*-derived spectral weights. As a consequence, the shoulder around −5.5 eV in the experiment is seen at −4.8 eV in the calculated DOS. Additionally, the Nb-4*d*-derived peak at −1.5 eV energy in the experimental spectra is shifted slightly closer to the Fermi level in the calculations. Such discrepancies are reminiscent of spurious *self-interaction* effects not sufficiently accounted for in conventional density-functional theory (DFT).

An approach to improve the orbital energies is to make use of hybrid functionals where an admixture of the exact Hartree-Fock exchange to conventional DFT functionals is incorporated [24,25]. We therefore have carried out such calculations by also varying the mixing parameter α [see Eq. (1)] from 0 to 0.30, applied not only to the Nb-4*d* states, but also to all electrons in the system. The optimal mixing parameter for Nb_3O_3 turned out to be 0.14, smaller than the standard value of 0.25 generally used for semiconducting or insulating 3*d*-TM oxides and perhaps not inconsistent considering the fact that niobium monoxide is a 4*d* system and a good metal too. The resulting Nb-4*d*, O-2*p*, and Nb-5*s* partial DOS are plotted in Fig. 2. The width of the VB using the hybrid functional is more extended than that of PBE-GGA and agrees better with the experimental spectra. The O-2*p*-derived shoulder around −5.5 eV, the Nb-4*d* peak around −1.5 eV, and the van Hove-like peak around −7.5 eV are reproduced precisely in our calculations. The hybrid-functional approach thus provides a highly accurate description of the valence-band spectrum.

We would like to note that the photoionization cross section for Nb-5*s* is tremendously enhanced when using the 6.5 keV light [32–34] with the result that the Nb-5*s* contribution to the valence band can be observed in the HAXPES spectrum, although the contribution by itself is tiny: We have enlarged the calculated Nb-5*s* partial density of states by a factor of 10 in Fig. 2 to make it visible. In Appendix we explain in more detail why Nb-5*s* does not play an important role for the physics of niobium monoxide.

B. Nb_3O_3 versus Nb_4O_4

It should be noted here that the presence of defect-free fcc Nb_4O_4 previously was deemed hypothetical already based on the finding that the Nb_3O_3 structure is more stable than the Nb_4O_4 structure by about 1 eV per NbO unit [15,16]. Also, the comparison of the DOS to the then available spectroscopic data supported this notion [14,18]. To confirm that such is still the case, even when considering *self-interaction* corrections, we performed hybrid-functional calculations for Nb_4O_4 as well with the same lattice constant $a = 4.21$ Å as Nb_3O_3. The resulting total and projected DOS are presented in Fig. 3: Indeed the DOS of Nb_4O_4 (middle panel) are very different

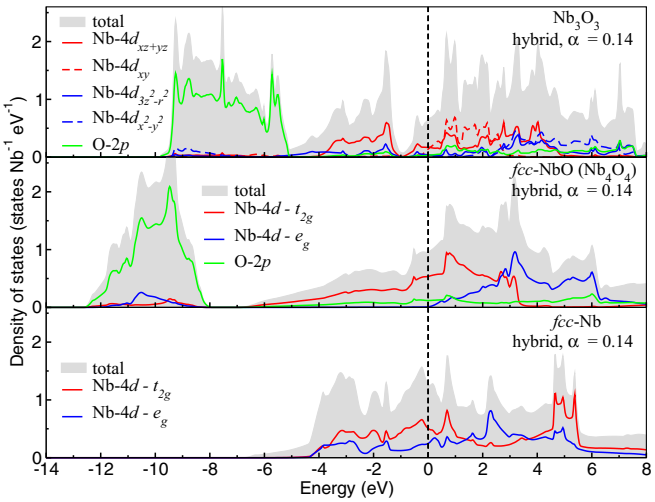

FIG. 3. Total and projected DOS for Nb_3O_3 (top panel) and the hypothetical fcc Nb_4O_4 (middle panel) using the screened hybrid functional with $\alpha = 0.14$. The bottom panel shows the DOS for the Nb metal in the fcc crystal structure. A lattice constant of $a = 4.21$ Å has been used for all three calculations.

from that of Nb_3O_3 or to our experimental VB spectra (Fig. 2), thus confirming the hypothetical nature of fcc Nb_4O_4. One immediate striking difference between the DOS of Nb_4O_4 and that of Nb_3O_3 is the much larger energy spread of the occupied DOS of Nb_4O_4, i.e., extending to −12.5 eV energy, whereas the DOS of Nb_3O_3 ends already at −10 eV. The fact that the O-2*p*-derived states in Nb_4O_4 extend to such a deep energy and become separated with a gap from the Nb-4*d*-derived states reflects the higher Madelung potential in the denser Nb_4O_4 structure. Therefore, the smaller Madelung energy of Nb_3O_3 must be (over)compensated by another electronic mechanism for the structure to be more stable.

The top and middle panels of Fig. 3 show a break down of the Nb-4*d* orbitals contributing to the VB. One clearly can observe that the e_g bands of the Nb_4O_4 structure are essentially above the Fermi level. In Nb_3O_3, the situation is quite different: Part of the e_g band, namely, $4d_{3z^2-r^2}$, is now extending well below the Fermi level. This constitutes a gain in the formation energy, and its origin has been discussed in the past in terms of a local cluster [10,12,35]. In Nb_4O_4, each Nb is octahedrally coordinated by six O ions, and the hybridization between them leads to a splitting of the Nb-4*d* levels into t_{2g} and e_g states. Since the π bonding for t_{2g} is significantly smaller than the σ bonding for e_g, the lowest Nb-4*d* states are derived from the t_{2g} states. With Nb having the formal 2+ valence and thus the $4d^3$ configuration, the occupied states then are made of only t_{2g}, whereas e_g's remain essentially unoccupied, see the middle panel of Fig. 3. In Nb_3O_3, Nb is locally square planar coordinated by four O ions. The lack of "apical" oxygens in this coordination makes that there is no σ bond for the $4d_{3z^2-r^2}$ orbital so that this state does not get pushed up in energy by the O-2*p*. Together with the large inter-4*d* hybridization, $4d_{3z^2-r^2}$ can develop bands, part of which is low enough in energy to become occupied [10–12,16,35,36], see the top panel of

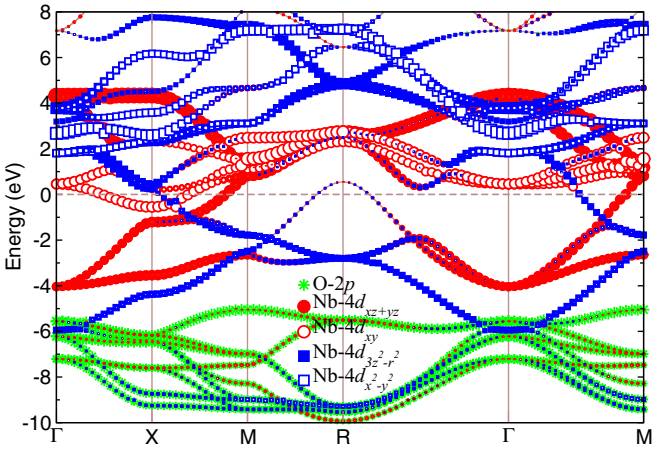

FIG. 4. Calculated band structure including the orbital character for Nb_3O_3 using the screened hybrid functional with $\alpha = 0.14$.

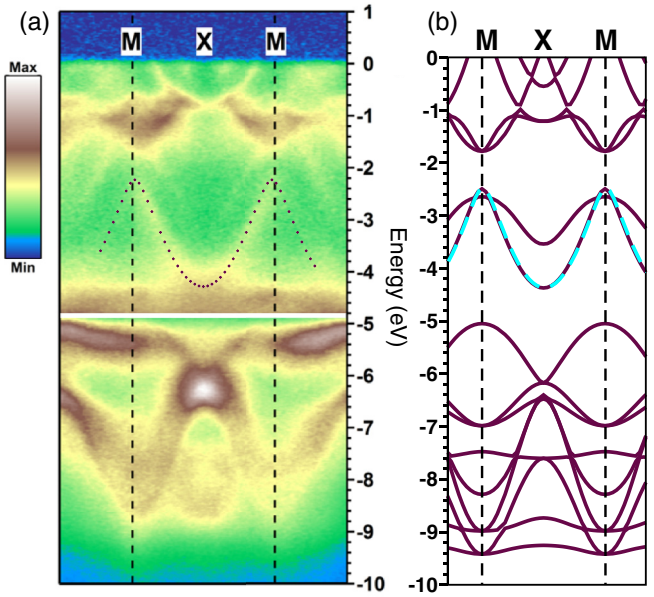

FIG. 5. (a) Experimental ARPES images along M-X-M with $h\nu = 168$ eV. (b) Calculated band structure along M-X-M using the screened hybrid functional with $\alpha = 0.14$. The 'vacancy' band is highlighted using the dotted and dashed lines in both panels.

Fig. 3. Obviously, with $4d_{3z^2-r^2}$ becoming partially occupied, t_{2g} should move up somewhat to conserve the number of electrons, but apparently this does not cost too much energy so that in the end there is a net gain of 1 eV per NbO unit [15,16] for Nb_3O_3 in comparison to Nb_4O_4.

It is important to note that the inter-4d hybridization is quite large. This can be illustrated by calculating the band structure of the fcc Nb metal with the same lattice constant as the hypothetical fcc Nb_4O_4. The results are presented in the bottom panel of Fig. 3. One can observe that both the Nb-4d t_{2g} and e_g bands have widths of roughly 9 eV. Such widths imply that correlation effects will not have a chance to stabilize magnetic or insulating states and that a nonmagnetic metallic solution for the ground states of Nb_4O_4 and Nb_3O_3 will be preferred. It is also precisely this large inter-4d bandwidth which allows for the partial filling of the $4d_{3z^2-r^2}$ band once it is not pushed up anymore to high energies by O-2p as Nb is in a local square planar symmetry in the Nb_3O_3 structure.

We would like to point out that the situation in 3d-transition-metal monoxides is quite different. We have calculated that, for example, the inter-3d bandwidth for fcc V with the VO lattice constant of $a = 4.073$ Å is about 4 eV and for fcc Ni with the NiO lattice constant of $a = 4.176$ Å is about 2 eV (see Appendix, Fig. 7). With such smaller one-electron bandwidths, electron correlation effects will manifest with the result that magnetic and insulating solutions can (and are) realized thereby reducing tremendously the effective or ARPES dispersions of the 3d-derived bands. Thus for 3d oxides one may very well need quite different energy considerations to explain the formation of defects which then also will have a more localized nature. A band-structure approach alone may not be adequate.

With the inter-4d bandwidth in niobium monoxide being very large, the interaction between the vacancies will also be long ranged so that ordering of the vacancies can be expected readily and, consequently, 'vacancy' bands are formed [14,16]. To illustrate this, we display in Fig. 4 the k-dependent band structure where we have put labels for the orbital characters of the various bands. These results are very similar to earlier studies [14,16,37,38] but with the difference that we used hybrid functionals with $\alpha = 0.14$ in order to have the best agreement with the experiment (Fig. 2). One clearly can see that below the Fermi level there are heavily dispersing bands with a predominantly Nb-$4d_{3z^2-r^2}$ character. These are the 'vacancy' bands of niobium monoxide [14,16].

C. Angle-resolved photoemission spectrum

Our next task is to show experimentally that these 'vacancy' bands indeed exist, and by that, to justify the band-structure approach for the understanding of the vacancy formation and ordering of the vacancies in niobium monoxide. Figure 5(a) depicts the experimental intensity image of the ARPES spectrum of niobium monoxide along the M-X-M path measured at $h\nu = 168$ eV (see Appendix, Fig. 8 for the experimental details). The dispersing features in the image can be grouped into three energy sections: (i) the electron and hole pockets spanning from E_F to -1.4 eV; (ii) one medium and one strongly dispersive band spanning -2 to -4.5 eV; (iii) a dense set of oxygen bands below -5 eV. Figure 5(b) displays the calculated band structure along the same M-X-M path. We can observe good general agreement between the measured and the calculated band structures. In all three energy sections mentioned above the band energy positions and dispersions are well reproduced. Of utmost relevance to our paper is the middle section where we can observe a dispersive band which we have highlighted using the dotted and dashed lines in Figs. 5(a) and

5(b). This is the Nb-4$d_{3z^2-r^2}$ 'vacancy' band as predicted by the band-structure calculations.

IV. SUMMARY

To summarize, we have performed angle-integrated and angle-resolved photoelectron spectroscopy measurements on niobium monoxide to investigate its electronic structure and the relationship with the vacancy-ordered crystal structure. We have established that band theory provides a good approach and can describe the valence-band features accurately by also taking into account corrections for *self-interaction* effects. The large inter-Nb-4*d* bandwidth plays an important role in the stabilization and ordering of the vacancies, and this is demonstrated clearly by the identification of the so-called 'vacancy' band in the experimental angle-resolved spectra.

ACKNOWLEDGMENTS

We thank A. A. Tsirlin for fruitful discussions and T. Mende for skillful technical assistance. D.K. gratefully acknowledges financial support from the DFG (deutsche forschungsgemeinschaft) through Project No. FOR 1346.

APPENDIX

1. The role of the Nb-5*s* states

In order to estimate the relative importance of the Nb-5*s* states for the electronic structure of Nb_3O_3, we have performed additional calculations by removing the 5*s* states from the basis set. To facilitate the calculation, we have used FPLO, a full-potential nonorthogonal local orbital code [39]. Figure 6 displays the band structure of Nb_3O_3 including (the orange lines) and excluding (the blue-green lines) Nb-5*s*. We can observe that the removal of Nb-5*s* does not cause bands

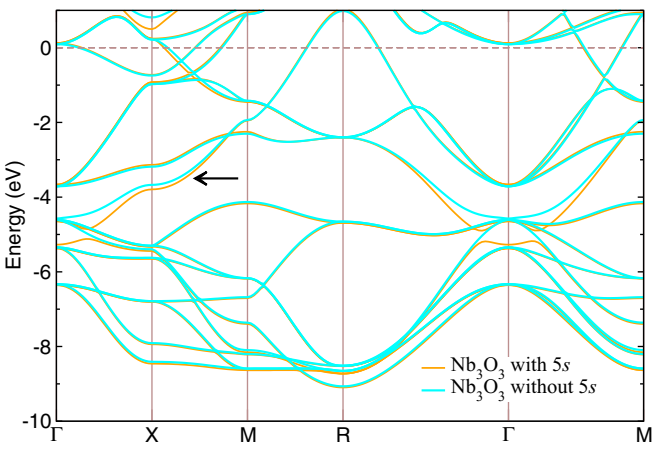

FIG. 6. Calculated band structure of Nb_3O_3 including (the orange lines) and excluding (the blue-green lines) the Nb-5*s* states. The arrow indicates the 'vacancy' band. See the text for details.

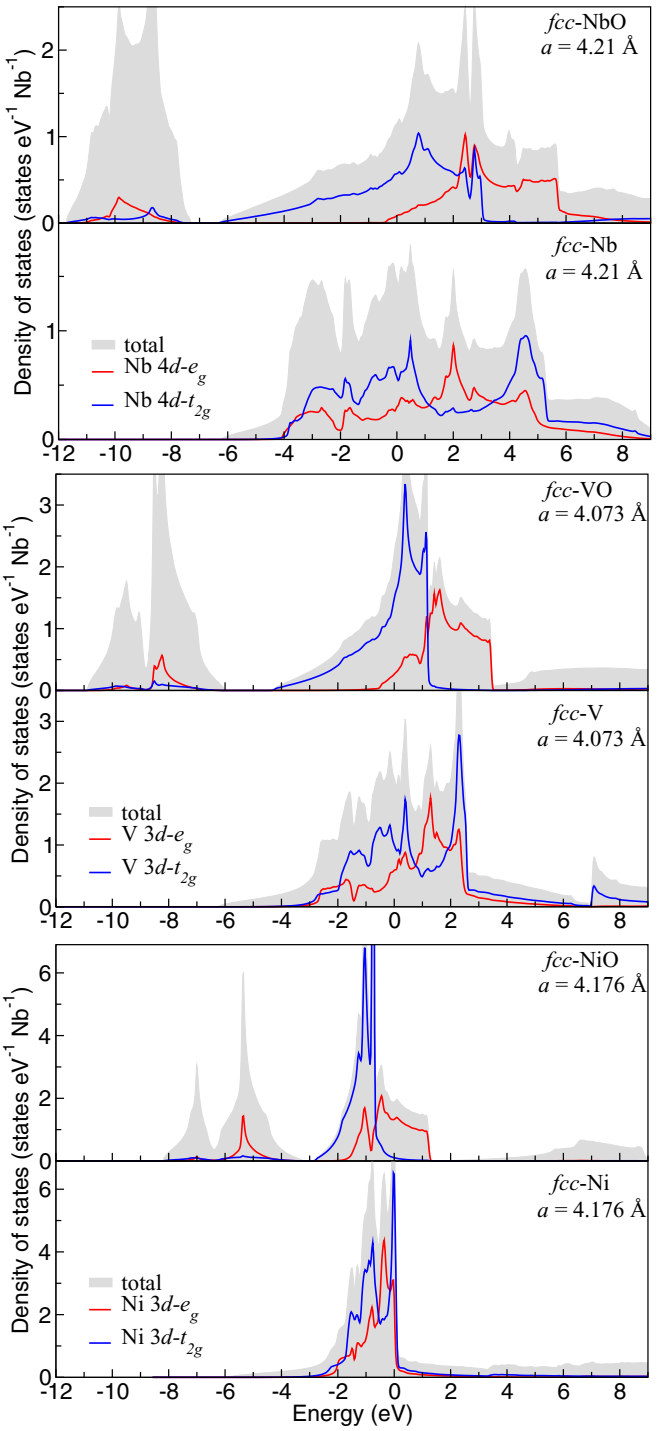

FIG. 7. Total and *d*-projected density of states for fcc NbO, Nb, VO, V, NiO, and Ni. The calculations were performed using the WIEN2K code and the PBE parametrization within the GGA.

to disappear in the occupied part of the band structure. In particular, the so-called 'vacancy' band (as indicated by the arrow) is still fully present. The removal of Nb-5*s* only causes small changes in the energy positions of some of the bands. We also have calculated the total energy of Nb_3O_3 including and excluding Nb-5*s*: The difference is 0.29 eV per formula

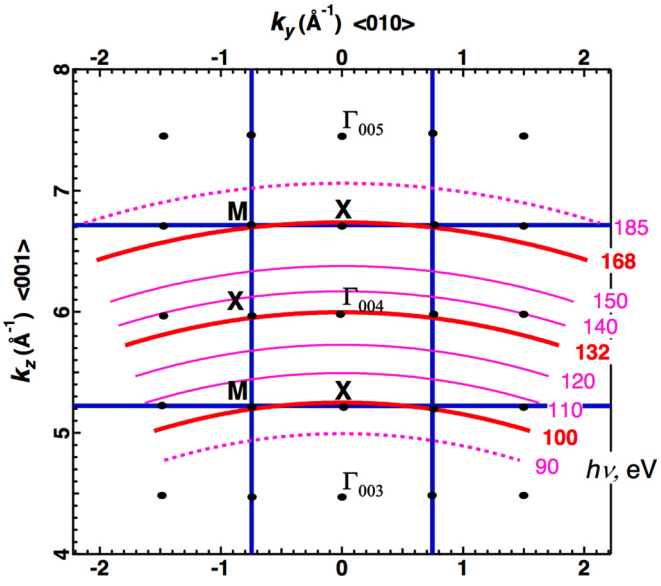

FIG. 8. Schematics of the experimentally probed cuts on the momentum space k_y-k_z plane with $k_x = 0$. The cuts are for photoelectrons with zero binding energy with the corresponding photon energies indicated. An inner potential of $V_0 = 9$ eV has been used. Cuts which pass through the high-symmetry points at normal emission are highlighted by the thick red lines. The electron energy analyzer has a $\pm 18^\circ$ angular acceptance with a work function of 3.87 eV.

unit. This is a modest amount when compared, for example, to the difference in the total energy of niobium monoxide in the Nb_3O_3 versus the Nb_4O_4 structure, which is about 1.3 eV per formula unit. We therefore can safely conclude that the Nb-5*s* states are playing only a minor role for the physics of niobium monoxide.

2. Inter-transition-metal *d* hybridization in rock-salt oxides

In order to estimate the inter-transition-metal hybridization strength in transition-metal 4*d* and 3*d* monoxide oxides with the rock-salt crystal structure, we calculate the band structure of fcc NbO/VO/NiO and fcc Nb/V/Ni with the same lattice constant as NbO/VO/NiO, respectively. See Fig. 7, which also includes the e_g and t_{2g} projections.

3. ARPES: momentum space mapping

The schematics of the momentum space mapping for the niobium monoxide ARPES experiment is depicted in Fig. 8. The sample is oriented with the [001] surface normal directed to the electron energy analyzer. An inner potential of $V_0 = 9$ eV has been used based on the extremal behavior observed in the energy dispersions of various Nb and O derived spectral features as a function of photon energy. A photon energy interval of 90–185 eV allows for the full coverage of the fifth Brillouin zone of niobium monoxide.

[1] H. Rose, Ueber das Niob, Annalen der Physik **180**, 310 (1858).

[2] G. Brauer, Die Oxyde des Niobs, Z. Anorg. Allg. Chem. **248**, 1 (1941).

[3] G. Andersson and A. Magnéli, Note on the crystal structure of niobium monoxide, Acta Chem. Scand. **11**, 1065 (1957).

[4] A. L. Bowman, T. C. Wallace, J. L. Yarnell, and R. G. Wenzel, The crystal structure of niobium monoxide, Acta. Crystallogr. **21**, 843 (1966).

[5] O. P. Kolchin and N. V. Sumarokova, The melting point and other properties of the lower oxides of niobium, At. Energ. **10**, 167 (1961).

[6] A. Taylor and N. J. Doyle, The thermal expansion of titanium, vanadium and niobium monoxides, J. Appl. Crystallogr. **4**, 103 (1971).

[7] A. Taylor and N. J. Doyle, Compressibilities and Grüneisen constants of the monoxides of titanium, vanadium and niobium, J. Appl. Crystallogr. **4**, 109 (1971).

[8] T. B. Reed, E. R. Pollard, L. E. Lonney, R. E. Loehman, and J. M. Honig, in *Inorganic Syntheses*, edited by A. Wold and J. K. Ruff (Wiley, New York, 1973), Vol. 14, pp. 131–134.

[9] A. D. Wadsley, in *Nonstoichiometric Compounds*, edited by L. Mandelcorn (Academic, New York/London, 1964), pp. 98–209.

[10] H. Schäfer and H. G. von Schnering, Metall-Metall-Bindungen bei niedrigen Halogeniden, Oxyden und Oxydhalogeniden schwerer Übergangsmetalle: Thermochemische und strukturelle Prinzipien, Angew. Chem. **76**, 833 (1964).

[11] J. K. Burdett and J. F. Mitchell, Nonstoichiometry in early transition metal compounds with the rocksalt structure, Prog. Solid State Chem. **23**, 131 (1995).

[12] O. K. Andersen and S. Satpathy, *in Basic Properties of Binary Oxides*, edited by A. D. Rodriguez, J. Casting, and R. Marquez (Servicio de Publicationes de la Universidad de Sevilla (Serie Ciencias), Sevilla, Spain, 1984), pp. 21–42.

[13] R. Chevrel and M. Sergent, in *Crystal Chemistry and Properties of Materials with Quasi-One-Dimensional Structures: A Chemical and Physical Synthetic Approach*, edited by J. Rouxel (Springer, Dordrecht, The Netherlands, 1986), pp. 315–373.

[14] E. Wimmer, K. Schwarz, R. Podloucky, P. Herzig, and A. Neckel, The effect of vacancies on the electronic structure of NbO, J. Phys. Chem. Solids **43**, 439 (1982).

[15] K. H. Schwarz, in *Basic Properties of Binary Oxides*, edited by A. D. Rodriguez, J. Casting, and R. Marquez (Servicio de Publicationes de la Universidad de Sevilla (Serie Ciencias), Sevilla, Spain, 1984), pp. 43–56.

[16] W. W. Schulz and R. M. Wentzcovitch, Electronic band structure and bonding in Nb_3O_3, Phys. Rev. B **48**, 16986 (1993).

[17] A. M. Okaz and P. H. Keesom, Specific heat and magnetization of the superconducting monoxides: NbO and TiO, Phys. Rev. B **12**, 4917 (1975).

[18] J. M. Honig, A. P. B. Sinha, W. E. Wahnsiedler, and H. Kuwamoto, Studies of the band structure of NbO by x-ray photoelectron spectroscopy, Phys. Status Solidi B **73**, 651 (1976).

[19] M. Erbudak, V. A. Gubanov, and E. Z. Kurmaev, The electronic structure of NbO: Theory and experiment, J. Phys. Chem. Solids **39**, 1157 (1978).

[20] W. W. Schulz, L. Forro, C. Kendziora, R. Wentzcovitch, D. Mandrus, L. Mihaly, and P. B. Allen, Band structure and electronic transport properties of the superconductor NbO, Phys. Rev. B **46**, 14001 (1992).

[21] J. Weinen, T. C. Koethe, C. F. Chang, S. Agrestini, D. Kasinathan, Y. F. Liao, H. Fujiwara, C. Schüßler-Langeheine, F. Strigari, T. Haupricht, G. Panaccione, F. Offi, G. Monaco, S. Huotari, K.-D. Tsuei, and L. H. Tjeng, Polarization dependent hard x-ray photoemission experiments for solids: Efficiency and limits for unraveling the orbital character of the valence band, J. Electron Spectrosc. Relat. Phenom. **198**, 6 (2015).

[22] P. Blaha, K. Schwarz, G. K. H. Madsen, D. Kvasnicka, and J. Luitz, *WIEN2K, An Augmented Plane Wave + Local Orbitals Program for Calculating Crystal Properties* (Karlheinz Schwarz, Technische Universität Wien, Austria, 2001).

[23] J. P. Perdew, K. Burke, and M. Ernzerhof, Generalized Gradient Approximation Made Simple, Phys. Rev. Lett. **77**, 3865 (1996).

[24] J. Heyd, G. E. Scuseria, and M. Ernzerhof, Hybrid functionals based on a screened Coulomb potential, J. Chem. Phys. **118**, 8207 (2003); **124**, 219906 (2006).

[25] J. Heyd and G. E. Scuseria, Efficient hybrid density functional calculations in solids: Assessment of the Heyd-Scuseria-Ernzerhof screened Coulomb hybrid functional, J. Chem. Phys. **121**, 1187 (2004).

[26] F. Tran and P. Blaha, Implementation of screened hybrid functionals based on the Yukawa potential within the LAPW basis set, Phys. Rev. B **83**, 235118 (2011).

[27] S. Hüfner, in *Photoelectron Spectroscopy: Principles and Applications* (Springer, Berlin/Heidelberg, 2003), pp. 173–209.

[28] J. A. Roberson and R. A. Rapp, Electrical properties of NbO and $PNbO_2$, J. Phys. Chem. Solids **30**, 1119 (1969).

[29] J. K. Hulm, C. K. Jones, R. A. Hein, and J. W. Gibson, Superconductivity in the TiO and NbO systems, J. Low Temp. Phys. **7**, 291 (1972).

[30] J. M. Honig, W. E. Wahnsiedler, and P. C. Eklund, Electrical properties of NbO in high magnetic fields, J. Solid State Chem. **6**, 203 (1973).

[31] J. Yeh and I. Lindau, Atomic subshell photoionization cross sections and asymmetry parameters: $1 \leqslant Z \leqslant 103$, At. Data Nucl. Data Tables **32**, 1 (1985).

[32] M. B. Trzhaskovskaya, V. I. Nefedov, and V. G. Yarzhemsky, Photoelectron angular distribution parameters for elements $Z = 1$ to $Z = 54$ in the photoelectron energy range 100-5000 eV, At. Data Nucl. Data Tables **77**, 97 (2001).

[33] M. B. Trzhaskovskaya, V. I. Nefedov, and V. G. Yarzhemsky, Photoelectron angular distribution parameters for elements $Z = 55$ to $Z = 100$ in the photoelectron energy range 100-5000 eV, At. Data Nucl. Data Tables **82**, 257 (2002).

[34] M. B. Trzhaskovskaya, V. K. Nikulin, V. I. Nefedov, and V. G. Yarzhemsky, Non-dipole second order parameters of the photoelectron angular distribution for elements Z = 1-100 in the photoelectron energy range 1-10 keV, At. Data Nucl. Data Tables **92**, 245 (2006).

[35] J. K. Burdett and T. Hughbanks, NbO and TiO: Structural and electronic stability of structures derived from rock salt, J. Am. Chem. Soc. **106**, 3101 (1984).

[36] J. K. Burdett and J. F. Mitchell, Pair potentials and the ordered defect structure of NbO, Inorg. Chem. **32**, 5004 (1993).

[37] Y. Kubo, S. Wakoh, and K. Schwarz, Theoretical momentum distributions in Nb_3O_3, J. Phys. Soc. Jpn. **55**, 1266 (1986).

[38] H. Aoki, Y. Asada, T. Hatano, K. Ogawa, A. Yanase, and M. Koiwa, Fermi surface of NbO, J. Low. Temp. Phys. **81**, 19 (1990).

[39] K. Koepernik and H. Eschrig, Full-potential nonorthogonal local-orbital band-structure scheme, Phys. Rev. B **59**, 1743 (1999).